Available online at www.sciencedirect.com

ScienceDirect

Geochimica et Cosmochimica Acta 327 (2022) 158–169

Geochimica et Cosmochimica Acta

www.elsevier.com/locate/gca

A nonlinear model for resolving the temperature bias of branched glycerol dialkyl glycerol tetraether (brGDGT) temperature proxies

Jiaju Zhao [a], Victor C. Tsai [b,*], Yongsong Huang [b]

[a] State Key Laboratory of Loess and Quaternary Geology, Institute of Earth Environment, Chinese Academy of Sciences, Xi'an 710061, China
[b] Department of Earth, Environmental and Planetary Sciences, Brown University, Providence RI 02912, USA

Received 16 July 2021; accepted in revised form 19 April 2022; Available online 26 April 2022

Abstract

Branched glycerol dialkyl glycerol tetraethers (brGDGTs) are a class of ubiquitous, bacteria-derived lipid biomarkers in terrestrial and aquatic environments. Many studies have demonstrated the potential for brGDGTs as paelotemperature proxies, but the observed seasonal bias in brGDGT-inferred temperatures still remains poorly understood, particularly for Arctic or seasonally dry climates. Here we introduce a new physical framework for understanding variations in the methylation index of branched tetraethers (MBT) by explicitly modeling the production and preservation of brGDGTs for a bacterial population with an exponential rate dependence on temperature. The dependence of MBT ratios on temperature is predicted to be nonlinear, and thus has a different form from other empirically defined MBT models. We apply the model to understanding how the methylation index depends on not only the mean annual air temperature (MAAT) but also how it depends on the amplitude of the seasonal temperature cycle and the phase and amplitude of the soil moisture content. We performed mesocosm growth experiments using natural lake waters that confirm that the model correctly accounts for lower brGDGT production rates during cold seasonal temperatures. Comparing the new model predictions with global compilations of MBT'_{5Me} and MBT' data, we determine a new calibration of best fitting set of model coefficients that more accurately account for the expected physical constraints on MBT-type data. Our new results account naturally for the expected saturation of MBT'_{5Me} and MBT' at low and high temperatures, a bias of up to 5–7 °C in MAAT for high seasonal temperature fluctuations, and an additional bias of up to 1–3 °C in MAAT for strongly seasonal soil moisture fluctuations. Taken together, the 3 effects explain differences of up to 15 °C in inferred MAAT compared with traditional empirical models for MBT'_{5Me} and MBT' and results in improved mean squared errors for both. At MAAT above 18 °C, MBT' temperature errors are lower than those of MBT'_{5Me}, suggesting MBT' may still be a useful proxy in some situations despite its added complexity. While we apply the framework only to global MBT'_{5Me} and MBT' proxy data, the physical framework can be adapted to other types of paleoproxies and may therefore be more widely applicable. Preliminary application of our model to the Pliocene North Sea Hank Core yields ~1 °C cooler temperatures than a previous calibration and application to 130 kyr-long Chinese Loess Plateau records yields ~4 °C warmer glacial and glacial stadial temperatures compared to previous calibration.

Keywords: brGDGT; Paleotemperature proxy; Physical model

1. INTRODUCTION

Understanding present and past climate variability is crucial for predicting future climate change. Quantitative

* Corresponding author.
E-mail address: victor_tsai@brown.edu (V.C. Tsai).

https://doi.org/10.1016/j.gca.2022.04.022
0016-7037/

paleoclimate information, such as paleotemperature, available at times prior to the availability of instrumental records are indispensable for evaluating the performance of climate models. Bacterial tetraether membrane lipids called branched glycerol dialkyl glycerol tetraethers (brGDGTs) are ubiquitous in both terrestrial and freshwater environments and have been successfully used to reconstruct past temperatures (e.g., Weijers et al., 2007; Tierney et al., 2010; Peterse et al., 2011, 2014; Gao et al., 2012; Jia et al., 2013; Lu et al., 2016, 2019; Tang et al., 2017; Inglis et al., 2020; Zhao et al., 2020; Zhao et al., 2021; Lauretano et al., 2021) and pH changes (e.g., Peterse et al., 2014; Lu et al., 2016; Fastovich et al., 2020; Sun et al., 2021). Numerous studies have documented empirical correlation between the ratios of various brGDGTs and mean annual air temperature (MAAT) in soils, lake sediments and peatland deposits across many different climatological and environmental gradients (e.g., Weijers et al., 2007; Loomis et al., 2012; Peterse et al., 2012; De Jonge et al., 2014; Naafs et al., 2017a,b; Dang et al., 2018; Russell et al., 2018). Various methylation indices for branched tetraethers (MBT, MBT', MBT'$_{5Me}$, MBT'$_{6Me}$) have been defined and shown to correlate with temperature, with most recent paleotemperature studies using MBT'$_{5Me}$ due to the sensitivity of other indices like MBT' to other environmental variables like pH (De Jonge et al., 2014).

However, brGDGT calibrations based on transects of environmental samples display relatively large root mean square errors (RMSEs) (±2–5 °C). More importantly, many regions display strong bias in brGDGT inferred temperatures, with inferred MAAT up to 10–20 °C warmer in lake sediments from Baffin Island (Shanahan et al., 2013) and 7 ± 1.4 °C warmer MAAT in animal bones from Alaska (Dillon et al., 2018), which are thought to reflect biased warm season production by bacteria in high latitude regions (e.g., Shanahan et al., 2013; Peterse et al., 2014; Dillon et al., 2018), though studies find minimal differences in samples collected in different seasons due to long turnover times of brGDGTs in soils (e.g., Weijers et al., 2011; Cao et al., 2018). In regions with hot/dry summers and relatively wet winters (e.g., the Mediterranean, the western USA), brGDGT inferred temperatures are up to 25 °C lower than MAAT (Peterse et al., 2012; Dirghangi et al., 2013; Menges et al., 2014), which has been attributed to preferential production during the cool, wet season. Menges et al. (2014) and Dang et al. (2016) suggest that in dry environments, water availability rather than temperature is the dominant control on methylation index. However, without a better understanding of this effect, it is difficult to correct potential seasonal bias in brGDGT-based temperature reconstructions, especially for paleoreconstructions, even after seasonal temperature variations have been taken into consideration (Dearing Crampton-Flood et al., 2020). The lack of mechanistic understanding, including not knowing the main producers of brGDGTs or the main ways in which environmental factors affect brGDGT production, has hampered validation of the proxy's use for paleotemperature reconstruction.

To better understand how seasonal temperature variability and soil moisture variability affect methylation index values (specifically MBT'$_{5Me}$ and MBT'), we introduce a simple physical framework for modeling the production and preservation of brGDGTs and apply the model to environmental conditions where temperatures have a known seasonality and soil moisture also has a known seasonal time dependence. Fitting the model parameters to a global database for MBT'$_{5Me}$ and MBT' measurements, we determine best-fitting parameters and demonstrate a significant saturation of MBT'$_{5Me}$ and MBT' at extreme temperatures, and a small but significant <5 °C bias in MAAT proxies when seasonal effects are not accounted for. Mesocosm experiments performed using natural lake samples grown in laboratory conditions confirm that the general form of the model is reasonable and suggest that all methylation index proxies may benefit from the proposed model.

2. GROWTH AND PRESERVATION MODEL FOR MBT-TYPE INDICES

The family of methylation indices that include MBT, MBT', MBT'$_{5Me}$, and MBT'$_{6Me}$ are all expressed as the ratio of certain brGDGT abundances and can generically be written as

$$P = \frac{C_1}{C_1 + C_2} \tag{1}$$

where P is one of the various methylation index proxies such as MBT'$_{5Me}$, and C_i is the abundance of some group of brGDGTs. For example, $MBT^{'} = (Ia + Ib + Ic)/(Ia + Ib + Ic + IIa + IIb + IIc + IIIa + IIa^{'} + IIb^{'} + IIc^{'} + IIIa^{'})$ so that in this case, we can associate $P = MBT'$, $C_1 = Ia + Ib + Ic$, and $C_2 = IIa + IIb + IIc + IIIa + IIa^{'} + IIb^{'} + IIc^{'} + IIIa'$. MBT'$_{5Me}$ can be defined similarly, without the accented terms. The premise of the proposed physical model is that the abundance observed in any particular soil or paleosol sample is the integrated effect of the rate of production of C_i over a timespan that is typically much longer than a single season and has a potentially nonlinear temperature dependence. Physically, this nonlinearity might be anticipated since rates of production are not expected to be negative for any temperature. For simplicity, we initially assume the simplest nonlinear temperature dependence, an exponential dependence, which implies

$$\frac{dC_i}{dt} = R_i(T(t)) = R_i^0 e^{A_i(T(t)-T_0)} \tag{2}$$

where R_i is the rate of production of C_i, $T(t)$ is the assumed known temperature as a function of time, A_i expresses the temperature dependence of R_i, and R_i^0 is the production rate at the arbitrary reference temperature T_0. (An exponential function is the simplest strictly increasing function that is always non-negative.) To calculate the predicted value of the proxy P, we integrate Eq. (2) for each C_i until a steady-state value of P is obtained through Eq. (1). As will be shown below, this simple setup has all of the ingredients needed to produce not only an expected temperature dependence of the proxy P, but also a bias in P as temperature cycles (e.g. seasonally).

To demonstrate the standard temperature dependence (e.g. dependence on MAAT), one can simply substitute a chosen fixed value of T_{MAAT} into Eq. (2) which then predicts that C_i increase linearly in time with different rates that depend on R_i^0 and A_i. Solving for the ratio gives

$$P(\Delta T) = \frac{R_1^0 e^{A_1 \Delta T}}{R_1^0 e^{A_1 \Delta T} + R_2^0 e^{A_2 \Delta T}} = \frac{1}{1 + \frac{R_2^0}{R_1^0} e^{(A_2 - A_1)\Delta T}} \tag{3}$$

where $\Delta T = T_{MAAT} - T_0$. From this result, we can already make a few interesting conclusions. Because P is expressed as a ratio which cannot be below zero or above one, P is best modeled as not being linearly dependent on ΔT but for $\log(\frac{1}{P} - 1)$ to depend linearly on ΔT (hereinafter, we use 'log' to refer to the natural logarithm with base e). Expressed in this manner, the y-intercept would be physically interpretable as $\log(R_2^0/R_1^0)$ and the slope would be physically interpretable as $A_2 - A_1$, which can be understood by rearranging Eq. (3) to solve for $\log(\frac{1}{P} - 1)$. If a more complicated model than the purely exponential model of Eq. (2) were used for the temperature dependence (see Supplementary Materials), then the proxy P is best modeled with

$$\log\left(\frac{1}{P} - 1\right) = m_0 + m_1 \Delta T + m_2 (\Delta T)^2 + m_3 (\Delta T)^3 + \cdots \tag{4}$$

where the m_i are various rate coefficients (see Supplementary Materials), and the ellipsis denotes higher order terms that could be included if additional accuracy were warranted. Since such rate coefficients may not be known, it may be most appropriate to determine them by fitting field data. The analysis in the Supplementary Materials demonstrates that any model with only positive production rates of brGDGTs results in a predicted ratio proxy P that must depend nonlinearly on temperature. For example, the fact that concentrations are positive already implies that P cannot be less than zero or greater than one, which Eq. (4) satisfies for all possible ΔT and m_i.

The role of a seasonally variable temperature on the proxy P can now be understood by assuming the temperature variability can be modeled as having an annual average (T_{MAAT}) plus a sinusoidal seasonal variability, $T(t) = T_{MAAT} + T_S \cdot \cos[\omega(t - t_0)]$, where T_S is the amplitude of the sinusoidal seasonal term, ω is the annual frequency ($2\pi/1\text{year}$), and t_0 accounts for the phase of the variability. Substituting this assumed $T(t)$ into Eq. (2) and integrating until a steady-state value of P is reached results in a steady state solution for Eq. (1) (see Supplementary Materials), which can be written as

$$P \approx \frac{R_1 I_0(A_1 T_S)}{R_1 I_0(A_1 T_S) + R_2 I_0(A_2 T_S)} = \frac{1}{1 + \frac{R_2}{R_1} I_0(A_2 T_S)/I_0(A_1 T_S)} \tag{5}$$

where I_0 is a mathematical special function known as a modified Bessel function (e.g., Arfken, 1985), and $R_i = R_i(T_{MAAT})$ accounts for the average MAAT. Since modified Bessel functions are somewhat obscure special functions, it is useful to note that a first approximation to the modified Bessel function is a purely quadratic function (see Supplementary Material), and using this approximation and adding it to Eq. (4) gives

$$\log\left(\frac{1}{P} - 1\right) = m_0 + m_1 \Delta T + m_2 (\Delta T)^2 + m_3 (\Delta T)^3 + m_S T_S^2 + \cdots \tag{6}$$

where m_S is the coefficient that expresses how strong the dependence on the squared amplitude of the seasonal temperature variability is expected to be. Importantly, the additional term $m_S T_S^2$ implies that the proxy P is sensitive to not only MAAT but also to how strong the seasonal fluctuations in temperature are. This in turn implies that models that do not include this additional dependence on T_S may be biased in their estimate of MAAT from P. As in Eq. (4), additional higher order terms could be included in Eq. (6) for T_S if additional accuracy were warranted. Including a seasonal bias term as in Eq. (6) whose form is derived from physical principles is expected to accurately account for seasonal production.

Finally, we note that the dependence of the MBT-type of proxy on other variables such as the cyclization of branched tetraethers ($CBT = -\log(\frac{Ib+IIb+IIb'}{Ia+IIa+IIa'})$) index (e.g., as a proxy for pH or other environmental conditions) (Weijers et al., 2007) or soil moisture content can also be included in this framework by simply assuming that R_i^0 has an extra dependence on the quantities of interest. As with Eqs. (3)–(6), since production rates are always positive, it can be shown that including these extra dependencies results in the same form of expected dependence, with the simplest assumption being that $\log(\frac{1}{P} - 1)$ depends linearly on the additional variables. Our final model for P can then be written as

$$\log\left(\frac{1}{P} - 1\right) = m_0 + m_1 \Delta T + m_2 (\Delta T)^2 + m_3 (\Delta T)^3 + m_S T_S^2 + m_{CBT} CBT + m_M M \tag{7}$$

where the mean annual air temperature (MAAT) dependence is determined by the three terms that depend on $\Delta T = T_{MAAT} - T_0$, the seasonal temperature dependence depends on the square of the amplitude of the seasonal temperature fluctuation T_S, and the dependencies on CBT and soil moisture proxy M are assumed to be as simple as possible. We note that using a different reference temperature T_0 would result in different values of m_i but that the functional form remains unchanged. Depending on how accurately the dependence of P on the various quantities are known, a larger or smaller number of terms may be used in the fit for that variable. In the global dataset that we analyze below, the MAAT dependence is more complex than can be accounted for with a single variable and thus warrants the 3-term fit (i.e., unknown parameters m_1, m_2 and m_3) whereas the fluctuations due to the other variables can be adequately fit with the corresponding 1-term fits as in Eq. (7). (Tests were done with more terms and found to only marginally lower the RMSE.) While the present paper focuses on MBT-type proxies, we note that the framework described here can also be applied to ratios of non-brGDGT species such as alkenones for which there is a nonlinear and seasonal temperature dependence.

Although applying this nonlinear framework to multivariable regression is beyond the scope of the present work, future extensions could be constructed to apply to multiple regression proxies like the MAT_{mr} proxy of De Jonge et al. (2014). We note, however, that the physical constraints emphasized in this work would result in a very different mathematical structure compared to purely statistical approaches such as in the recent Vequaud et al. (2022) study, which has some of the same limitations as the linear empirical models described above. It is difficult to know when such statistical constraints are reliable when applied in situations that are different from those in the calibration dataset.

3. LABORATORY EXPERIMENTS TO CONFIRM MODEL FRAMEWORK FOR TEMPERATURE DEPENDENCE

Prior to applying the framework discussed in Section 2 to field data, we first confirm that brGDGTs and the MBT'_{5Me} and MBT' proxies specifically have a temperature dependent growth rate that are adequately described by the framework defined above. We accomplished this by performing mesocosm laboratory experiments in which natural lake samples from under ice cover at Lake Wudalianchi (~0 °C) were kept under normal aerobic conditions for 11 months but with a range of natural and unnatural temperature conditions, with brGDGT analyses being done on samples every 4 weeks (Fig. 1; see Supplementary Materials for details about the extraction protocol, separations and mass spectrometer analyses). The temperature cycling was such that temperature rose slowly for the first ~5 months (approximately +1.62 °C/month), decreased more rapidly over the next ~3 months (approximately −4.2 °C/month), and then was maintained at a cold ~4 °C for another 2 months (see Fig. 1). MBT' and MBT'_{5Me} were calculated using the standard methodology (Peterse et al. 2012; De Jonge et al., 2014). As shown in Fig. 1, the MBT'_{5Me} and MBT' proxies show the expected increase with warm/warming temperatures and a decrease in the proxies with cold/cooling temperatures. However, it is also clear that when temperature is held roughly constant, there is a lag in the proxies, with MBT'_{5Me}/MBT' increasing during steady warm temperatures, and MBT'_{5Me}/MBT' decreasing by a smaller amount during steady cold temperatures. As expected, this implies that the measured value of MBT'_{5Me}/MBT' cannot depend only on the instantaneous temperature, and strongly suggests that it is instead the rate of change of the individual constituent brGDGTs that is affected by temperature, as described in Eq. (2).

To further test the applicability of the modeling framework described in Section 2, we fit the laboratory data with a version of the model modified to account for the very short timescale of the experiments. Different from natural samples, the temperature variability in the ~1-year laboratory experiment time period is not long enough to reach the steady-state solution in Eq. (5). However, one can still numerically integrate Eq. (2) given the known laboratory temperature time series $T(t)$ and determine the coefficients R_i^0 and A_i that allow the modeled MBT'_{5Me}/MBT' to best

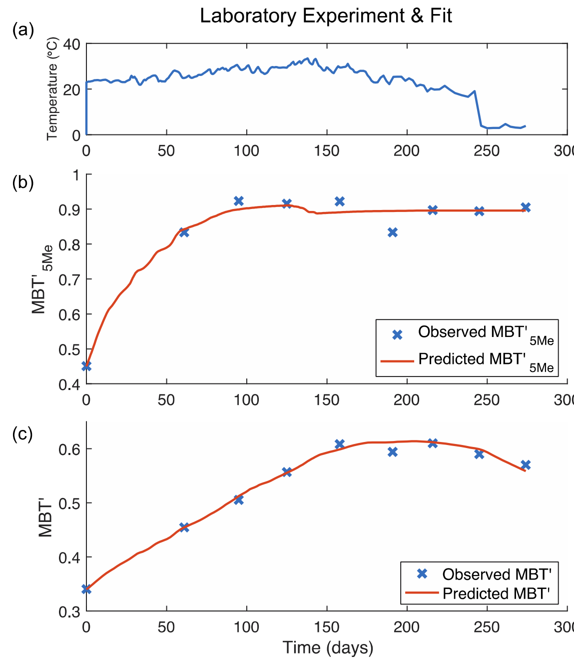

Fig. 1. Laboratory experiment data and model fit. (a) Imposed temperature vs. time, (b) Observed MBT'_{5Me} values (blue crosses) and predicted MBT'_{5Me} values for the best fitting model with parameters $R_1^0 = 6.0$/day, $R_2^0 = 0.08$/day, $A_1 = 0.45$/°C, $A_2 = 0.65$/°C, $T_0 = 20$ °C. (c) Same as (b) for MBT' with parameters $R_1^0 = 4.2$/day, $R_2^0 = 4.5$/day, $A_1 = 0.1$/°C, $A_2 = -0.05$/°C, $T_0 = 20$ °C.

fit the measured MBT'_{5Me}/MBT' values. Performing a grid search over the parameters yields a model that reasonably accurately fits the MBT'_{5Me}/MBT' data (see Fig. 1). The success of the model in capturing the laboratory observations provides encouraging support that the model framework may also appropriately capture the temperature variability observed at field sites around the world. Although the best fitting laboratory parameters are unlikely to be relevant to field conditions, they confirm that the nonlinear temperature dependent production rate assumed in Eq. (2) is consistent with the laboratory data and motivates the attempt to use the framework at a global scale with model constraints from field data. We note that the MBT'_{5Me} data initially increase more quickly than in the MBT' case and is modeled to do so because the temperature dependence is stronger (coefficients A_1 and A_2 are larger), resulting in more production when temperature is suddenly increased from 0 °C.

4. GLOBAL CALIBRATION OF THE NEW MODEL FOR MBT'_{5ME} AND MBT'

To determine the best-fitting parameters of the new model in field conditions, particularly with the aim of constraining the best MAAT dependence, the best seasonal temperature dependence, and the role of soil moisture, we fit Eq. (7) to a global database of 561 MBT'_{5Me}, MBT' and CBT measurements (Peterse et al., 2012; De Jonge et al., 2014; Wang et al., 2016; Naafs et al., 2017a; Dearing Crampton-Flood et al., 2020). For each site, daily average temperature measurements (CHELSA database version 2.1, Karger et al., 2017) were used to determine the best-fitting sinusoid, i.e. $T(t) = T_{MAAT} + T_S\cos(\omega t + \phi)$, where $\omega = 2\pi/(1\text{year})$ and ϕ is the phase of the seasonal variability. Similarly, monthly soil moisture measurements (TerraClimate database, Abatzoglou et al., 2018) were used to determine the amplitude and phase of the moisture content variability. To reduce the weight in the calibration to densely sampled regions, we average individual site data at a grid resolution of 0.5 degrees. (See Supplementary Table 1 for the data at the 561 individual sites as well as the mean data for the 235 geographically averaged sites used in this study.) Here we choose to define the moisture content proxy M as the projection of the seasonal moisture content (precipitation minus evaporation in mm) variability onto the seasonal temperature variability, so

$$M = \frac{\vec{T}_S \cdot \vec{M}_S}{T_S} \tag{8}$$

where $\vec{T}_S$ is the vector seasonal temperature and $\vec{M}_S$ is the vector seasonal moisture (see Supplementary Material). We note that with this definition, M has units of mm equivalent water, and is positive when moisture content correlates strongly with temperature and is negative when moisture content anticorrelates with temperature. This choice emphasizes the role that the relative phase and amplitude of the seasonally varying moisture content might have in affecting MBT'$_{5Me}$/MBT'. Other choices of M are possible and would be appropriate for different hypotheses regarding how moisture potentially affects brGDGT production and thus MBT'$_{5Me}$/MBT' measurements. In Fig. 2, we plot the MBT'$_{5Me}$ and MBT' data (symbol size) vs. MAAT and seasonal T_S, and colored by M. While we have used the entire global database for this calibration study, calibration could be improved for specific environmental conditions at the cost of having fewer data points (e.g., Russell et al., 2018; Raberg et al., 2021) and could be done in future work. While most recent paleotemperature studies have focused on MBT'$_{5Me}$, due to its lower sensitivity to pH and generally lower residual errors than other MBT-type proxies, we have chosen to also provide global calibrations for the older MBT' proxy since an improved calibration for it could revive its usefulness despite its more complex dependence on other environmental variables compared with MBT'$_{5Me}$.

With all the variables in Eq. (7) measured for the global dataset, we can proceed to determining the best-fitting coefficients m_0, m_1, m_2, m_3, m_S, m_{CBT}, and m_M. We perform a least-squares fit of the transformed data $\log(\frac{1}{P} - 1)$ (where P = MBT'$_{5Me}$ or MBT') to solve for the 7 unknown parameters. To maintain the expected monotonic dependence of MBT'$_{5Me}$/MBT' on MAAT, we force monotonicity for the ΔT dependence in Eq. (7) over the range -10 °C < T < 30 °C, which can be expressed as algebraic inequalities on m_1, m_2 and m_3 (Fenimore et al., 2000). The best fitting parameters are tabulated in Table 1 (MBT'$_{5Me}$ parameters in row 1, MBT' parameters in row 2). The predicted

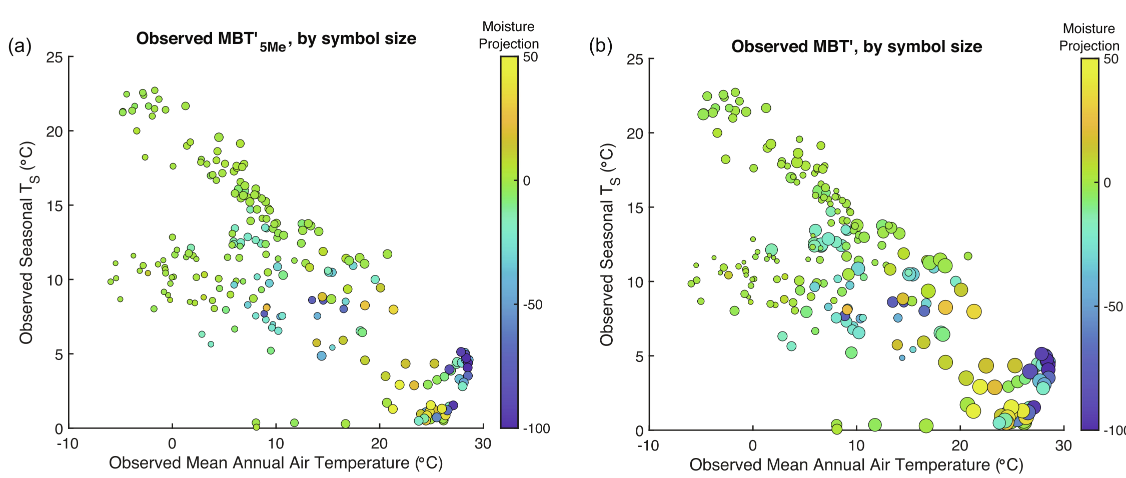

Fig. 2. (a) Observed MBT'$_{5Me}$ (symbol size) as a function of mean annual air temperature (MAAT) (x axis) and seasonal temperature variability T_S (y axis), colored by moisture proxy M. (b) Same as (a) for MBT'. We note that most sites with MAAT lower than 0 °C and below 15 °C T_S are either in the coastal Arctic or the Tibetan Plateau. To account for the different mean values, symbol sizes in (a) are 75MBT'$_{5Me}$ points and in (b) are 200MBT' points.

Table 1
Model parameter values, with T_0 = 10 °C. Units are degrees C for temperature, unitless for MBT'$_{5Me}$, MBT' and CBT, and mm equivalent water for moisture content. Thus, units for m_1 are 1/°C and units for m_2 and m_S are 1/(°C)^2.

	T_0	m_0	m_1	m_2	m_3	m_S	m_{CBT}	m_M
MBT'$_{5Me}$	10 °C	−0.2061	−0.1336	-2.21×10^{-3}	1.89×10^{-5}	-1.84×10^{-3}	−0.365	-7.59×10^{-3}
MBT'	10 °C	1.6058	−0.1074	-2.73×10^{-3}	-1.57×10^{-6}	-7.93×10^{-4}	−1.254	-4.52×10^{-3}

MBT'$_{5Me}$ is plotted with the observed MBT'$_{5Me}$ as a function of MAAT in Fig. 3a and the predicted MBT' is plotted with the observed MBT' as a function of MAAT in Fig. 3c. Residuals are plotted in Fig. 3b and d, respectively. To compare the new model results with previous calibrations, the linear regression calibrations of De Jonge et al. (2014), Naafs et al. (2017a) and Dearing Crampton-Flood et al. (2020) are plotted in Fig. 3a and the linear regression calibration of Peterse et al. (2012) is also plotted in Fig. 3c (using average CBT), with residuals for all models also shown in Fig. 3b and d.

Root-mean squared error (RMSE) for our new calibrations are lower than the corresponding linear models, with a RMSE of 0.090 (in non-dimensional proxy ratio units) for the new nonlinear MBT'$_{5Me}$ calibration, compared with 0.169 for the De Jonge linear MBT'$_{5Me}$ model, 0.119 for the Naafs linear MBT'$_{5Me}$ model and 0.104 for the Dearing Crampton-Flood median BayMBT MBT'$_{5Me}$ model (see Fig. 3b), and a RMSE of 0.139 for the new nonlinear MBT' calibration, compared with 0.186 for the Peterse linear MBT' model (see Fig. 3d). For the MBT'$_{5Me}$ linear models, we note that the De Jonge and Naafs models both have positive residuals at low MAAT and negative residuals at high MAAT; in contrast, the Dearing Crampton-Flood model has positive residuals at moderately high MAAT (15–25 °C) and slightly negative residuals at low MAAT (<5°C), suggesting that purely linear models do not fully capture the observed trends despite capturing the linear portion of the trends. Since the new models are nonlinear, the reported RMSEs in MBT'$_{5Me}$ and MBT' correspond to different MAAT RMSEs depending on the values of MAAT or the proxies. For example, the same 0.090 RMSE for MBT'$_{5Me}$ corresponds to a 2.9 °C RMSE at a MAAT of 10 °C, a 3.3 °C RMSE at a MAAT of 5 °C and a 5.2 °C RMSE at a MAAT of 20 °C; and the 0.139 RMSE for MBT' corresponds to a 5.5 °C RMSE at a MAAT of 10 °C, a 8.8 °C RMSE at a MAAT of 5 °C and a 4.0 °C RMSE at a MAAT of 20 °C. There is also structure in the error, for example with generally smaller residuals (and thus RMSE) from 18–27 °C (and also −5 to 4 °C to a lesser extent) than from 5–17 °C (see blue circles in Fig. 3b and d), so that one may expect lower MBT'$_{5Me}$ error at temperatures at 18–27 °C than one would calculate with the global RMSE. We also note that while most recent authors have favored the MBT'$_{5Me}$ proxy to the MBT' proxy because models for it have a reduced RMSE and have a less significant pH dependence, our new MBT' calibration has a lower RMSE compared to the De Jonge MBT'$_{5Me}$ model and has a lower MAAT RMSE than our MBT'$_{5Me}$ calibration for some temperatures, suggesting that there may be situations where MBT' may still provide useful MAAT constraints. For example, due to the earlier saturation of MBT'$_{5Me}$ at high temperatures compared to MBT' (approaching values near 1 at lower temperatures),

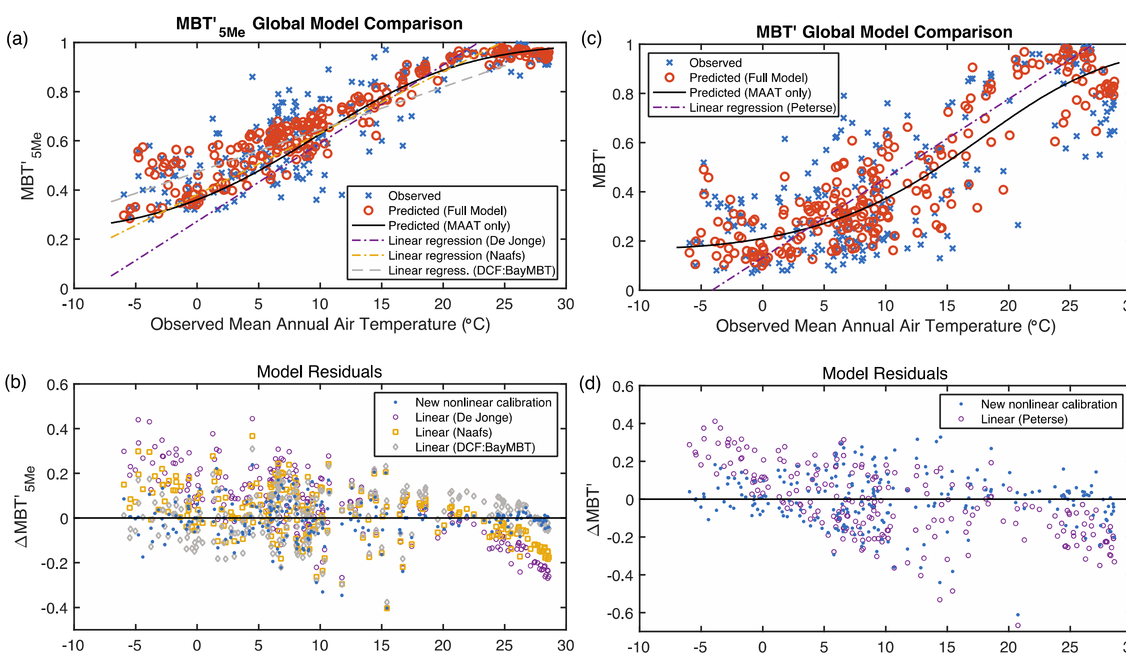

Fig. 3. Comparisons of observations and predictions for global datasets. (a) Observed MBT'$_{5Me}$ (blue crosses) and predicted MBT'$_{5Me}$ (red circles) as a function of observed mean annual air temperature (MAAT). Black line denotes the average MAAT dependence of the model. Purple dashed-dotted line denotes the linear regression model of De Jonge et al. (2014), the yellow dashed-dotted line denotes the linear regression model of Naafs et al. (2017a) and the gray dashed line denotes the median linear regression model BayMBT of Dearing Crampton-Flood et al. (2020). (b) Residual plot of observed MBT'$_{5Me}$ minus predicted MBT'$_{5Me}$ as a function of MAAT. Filled blue circles are for the new nonlinear model calibration, open purple circles are for the De Jonge et al. (2014) linear model, open yellow squares are for the Naafs et al. (2017a) linear model and open gray diamonds are for the median BayMBT linear model. (c) Same as (a) for MBT'. Purple dashed-dotted line denotes the linear regression model of Peterse et al. (2012). (d) Same as (b) for MBT'. Open purple circles are for the Peterse et al. (2012) linear model.

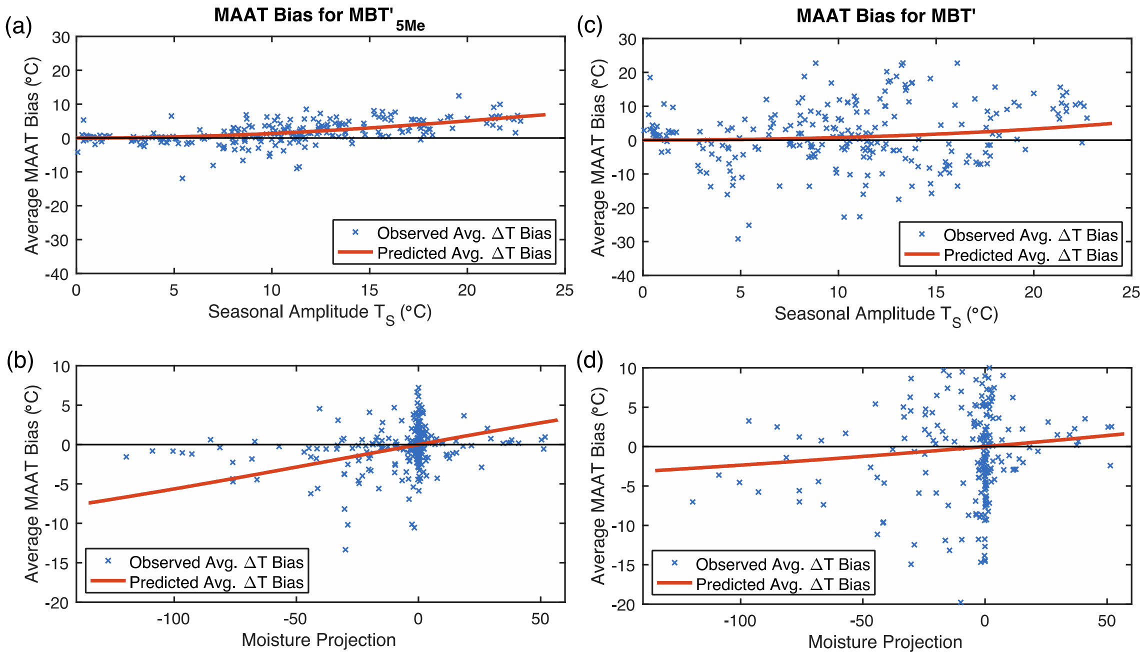

Fig. 4. (a) Observed MBT'$_{5Me}$ minus predicted MBT'$_{5Me}$ excluding the T_S term, converted to predicted average temperature bias assuming an average temperature of 10 °C (blue crosses). Red line shows the predicted bias from the model, converted to average temperature bias in the same way. (b) Observed MBT'$_{5Me}$ minus predicted MBT'$_{5Me}$ excluding the M term, converted as in (a) (blue crosses). Red line is the predicted bias. (c) Same as (a) for MBT'. (d) Same as (b) for MBT'.

the mean 0.139 RMSE for MBT' results in a lower MAAT RMSE than the 0.090 RMSE for MBT'$_{5Me}$ at temperatures higher than 18 °C, with a MAAT RMSE of 4.0 °C for MBT' and a MAAT RMSE of 5.2 °C for MBT'$_{5Me}$ at a MAAT of 20 °C. Thus, the MBT' proxy may provide higher resolution of warm paleoclimates than MBT'$_{5Me}$ despite the fact that it has a more complicated dependence on other environmental factors.

The value of m_S implies that for a large 20 °C seasonal temperature fluctuation ($T_S = 20$), there is a −0.736 bias in $\log(\frac{1}{P} - 1)$ for MBT'$_{5Me}$ and a −0.317 bias in $\log(\frac{1}{P} - 1)$ for MBT'. The amount of bias predicted in MBT'$_{5Me}$ or MBT' depends on its background value. For example, for a background value of MBT'$_{5Me}$ = 0.8, the seasonal bias in MBT'$_{5Me}$ is predicted to be +0.093 whereas for a background value of MBT'$_{5Me}$ = 0.4, the same 20 °C seasonal fluctuation causes a predicted bias in MBT'$_{5Me}$ of +0.182. The bias is shown graphically for MBT'$_{5Me}$ and MBT' in Fig. 4a and c, respectively, by plotting the observed values minus the predicted values excluding the seasonal temperature term (T_S) as a function of T_S, converted into a predicted average temperature bias assuming an average temperature of 10 °C. Plotted as a red line is the predicted average bias of the model. As shown, at the most extreme seasonal temperatures (T_S > 20 °C), there is a robust bias in predicted MAAT of about 7 °C for MBT'$_{5Me}$ and a somewhat smaller but still robust bias of about 5 °C for MBT'. Thus, we expect locations with large seasonal temperature variability to have MBT'$_{5Me}$ or MBT'-inferred MAAT up to 5–7 °C too high if the seasonal term were not included.

Performing a similar analysis for the bias due to moisture content, the maximum bias in predicted MAAT is about 3 °C for MBT'$_{5Me}$ and about 1 °C for MBT'. Unfortunately, the bias due to moisture content is not as well constrained as the seasonal temperature bias with the global dataset, partly because the majority of the data occur at small magnitudes of moisture projection (|M|<10 mm), with an uncertainty in the bias that often exceeds the bias itself (see Fig. 4), and partly because the coarseness of the global moisture database does not accurately capture small-scale moisture variability. This bias is perhaps only important for sites where moisture content is strongly variable and either correlates or anticorrelates strongly with temperature, and should be revisited in later work if a more robust relationship is needed than is possible to constrain with the present data and model. Potential users of the model may assume the m_M coefficient is zero if they do not want to include this moisture part of the model and the rest of the model remains unchanged. Additionally, if more accurate moisture data become available in the future, it would be straightforward to recalibrate this part of the model.

As described in Eq. (7), we also test the inclusion of CBT as an explanatory variable, despite recent calibrations suggesting that MBT'$_{5Me}$ is uncorrelated with pH (De Jonge et al., 2014). Consistent with previous findings, we find that CBT explains a large and significant bias in MBT' of about +13 °C per CBT unit (i.e., +13 °C/1CBT). However, we also find that CBT explains a smaller (but still significant) bias in MBT'$_{5Me}$ of about +2.6 °C per CBT unit, the smaller bias being consistent with previous findings that pH does not correlate significantly with MBT'$_{5Me}$. To further test the robustness of this result, we check whether the fractional cyclization index fC (Martinez-Sosa and Tierney, 2019) has a similar effect when included in place of CBT. We find a significant negative MAAT bias for fC (-1.8 °C per 0.1 fC units at a mean of 10 °C) in the MBT'$_{5Me}$ calibration, consistent with the (positive) CBT bias for MBT'$_{5Me}$. We do not attempt to explain the reason that CBT remains a statistically significant explanatory variable for MBT'$_{5Me}$ despite the lack of correlation between MBT'$_{5Me}$ and pH, but advocate keeping it in the calibration due to its significant explanatory power.

We close this section by describing how users may utilize the nonlinear models with parameters listed in Table 1 to infer MAAT given measurements of the proxy (e.g., either MBT' or MBT'$_{5Me}$). Due to the nonlinear nature of the model, inverting Eq. (7) to solve for ΔT in terms of measured P, T_S, CBT and M is not as straightforward as with purely linear models. The easiest way of utilizing the new calibration is to calculate the ΔT-dependent terms on the right hand side (RHS) of Eq. (7) for all possible ΔT (e.g., all temperatures between −10 °C and 30 °C) and then use this as a look-up table to find the ΔT that best matches LHS = RHS for the specific measured values of the proxy P, T_S, CBT and M at each site. Since the model is constrained to be monotonic in ΔT, the inferred ΔT is unique. Code to perform this inversion is provided in the Code Availability section.

5. APPLICATION TO MBT PALEOSOL TEMPERATURE PROXIES

Many studies have shown that high latitude sites have brGDGT-inferred temperatures that are substantially higher than mean annual averages (e.g., Pearson et al., 2011; Weijers et al., 2011; Shanahan et al., 2013; Wang et al., 2016; Naafs et al., 2017a; Dang et al., 2018). Our new physical model implies that such a bias is expected for two reasons. First, and most importantly, as shown in Fig. 3a, the physical model demonstrates that MBT'$_{5Me}$ and MBT' (or other ratio-based proxies) cannot maintain their linear relationship with MAAT for extreme temperatures due to the physical impossibility of negative ratios of observed quantities (or ratios above 1). For example, the Naafs et al. (2017a) calibration predicts MBT'$_{5Me}$ = 1.006 at a MAAT of 25 °C, which is impossible. Accounting for a physical model implies that MBT'$_{5Me}$ values at low MAAT (below ~10 °C) will be higher than would have been predicted using a linear fit (by up to +0.2 in MBT'$_{5Me}$ and up to +10 °C in inferred MAAT for very low MAAT) and vice versa for high MAAT (above 20 °C); similarly, MBT' values at low MAAT (below ~4 °C) from the Peterse linear fit are biased low, with the new model predicting up to +0.3 MBT' and +10 °C for low MAAT, and vice versa for high MAAT (above 22 °C). This therefore explains a significant part of the trend towards higher MBT'$_{5Me}$/MBT' values and higher inferred temperatures at sites with MAAT < 10 °C. We note that the linear calibration of Dearing Crampton-Flood et al. (2020) appears to partially fix this extreme temperature bias but at the cost of degrading the RMSE at intermediate temperatures (data from 15 to 25 °C appear to be biased high compared with the model, with significantly worse fit in this temperature range; see Fig. 3ab), whereas the nonlinear model has lower RMSE residuals over a wider range of temperatures.

The nonlinear nature of the new model also leads to significant differences compared to the linear model at intermediate temperatures, especially for the MBT' results. As shown in Fig. 3b, the new nonlinear model has significant curvature in the MBT'/MAAT relationship, with the new predicted MBT' values being offset to lower values than predicted with the linear regression model of Peterse et al. (2012) (in other words, a given value of MBT' predicts higher MAAT). This intermediate temperature offset is less severe for the new MBT'$_{5Me}$ calibration primarily because the global data are more linear over the observed range of temperatures and quite closely follows the Naafs et al. (2017a) calibration for temperatures between 0–20 °C (although it is sometimes more than 1 °C different), with more significant differences only at more extreme temperatures. The nonlinearity of the model generally implies that a given change in MAAT has a greater effect on MBT'$_{5Me}$/MBT' values at intermediate temperatures than at more extreme temperatures.

A second significant bias is due to generally higher rates of production of brGDGTs during warmer seasons. Thus, for sites with low MAAT but a strong seasonal temperature variability (upper left of Fig. 2ab), we predict a strong bias in MBT'$_{5Me}$ of up to +0.23 or an inferred MAAT bias of up to about 7 °C (see Fig. 4a) and a weaker bias in MBT' of up to +0.10 or an inferred MAAT bias of up to about 5 °C (see Fig. 4c). In contrast, for sites with low MAAT but small seasonal temperature variability (lower left of Fig. 2a), we predict there to be no significant additional bias from seasonal variability. Including both the nonlinearity and seasonality effects, the new physical model predicts up to a 15 °C difference compared to a linear model without a seasonal term for the coldest and most seasonally variable sites for both MBT'$_{5Me}$ and MBT'.

In addition to temperature, soil moisture also plays an important role in determining the production of brGDGTs in soils. Previous studies suggested that soil brGDGT-inferred temperatures are significantly lower than MAAT for sites with dry summers, such as the Iberian Peninsula, the Mediterranean and Arizona (Peterse et al., 2011; Menges et al., 2014; De Jonge et al., 2014). Our model suggests that there can be a bias of up to 3 °C for MBT'$_{5Me}$ and up to 2 °C for MBT' due to soil moisture being highly variable and anticorrelated with temperature variability (i.e. wetter cold season; see Fig. 4bd). It is likely that a different soil moisture proxy that better accounts for the severity of the dry season may produce a stronger bias and thus be better able to explain the large observed bias, but such a proxy was not identified and could be the topic of future study. We note that when the dry season is extreme, the physical model represented by Eq. (7) with a linearly added moisture proxy term may also be too simplistic, and the modeling framework should be revisited to specifically account for this physics.

As an initial demonstration of the competing temperature biases for MBT'$_{5Me}$, we apply our new nonlinear calibration to the Hank Core Pliocene marine sediment sequence in northwestern Europe (North Sea basin), which has been analyzed by Dearing Crampton-Flood et al. (2020). For T_S and M, we use modern estimates, though future work could potentially improve upon this by using paleoclimate simulations; future work will also be needed to determine more generally which locations and paleoclimates have seasonal fluctuations that are similar to modern estimates or not. In Fig. 5 we show paleotemperature estimates using our revised nonlinear calibration (thick blue line), compared with estimates using previous calibrations (De Jonge et al. (2014), Naafs et al. (2017a), and Dearing Crampton-Flood et al. (2020)) as well as a version of our nonlinear calibration with only the MAAT dependence included (no seasonal or moisture correction; thick dashed red line). Interestingly, for this profile, the nonlinear bias, seasonal bias and moisture bias are all significant (each with > 1 °C predicted differences). The seasonal bias is moderate, with a seasonal temperature variability of T_S = 7.1 °C, corresponding with near-Arctic European coastal conditions. The moisture bias is strong and negative, with M = −23.9 mm, corresponding to wet winter and dry summer conditions. The combination of the nonlinear bias and moisture bias results in the Hank Core estimated MAAT being significantly higher than that using the Naafs et al. (2017a) calibration by an average of +2.5 °C, despite the moderate seasonal bias in the opposite direction. Our estimated MAAT is lower than that predicted by the BayMBT$_0$ calibration of Dearing Crampton-Flood et al. (2020) by an average of −1.0 °C. We suggest that the inferred temperatures of Dearing Crampton-Flood et al. (2020) may be slightly overestimated due to the bias in intermediate temperatures discussed at the beginning of this section, but their estimates are also affected by their choice of priors. The fact that our estimated MAAT is fairly similar to that predicted by the De Jonge et al. (2014) calibration is somewhat fortuitous, due to multiple corrections partially

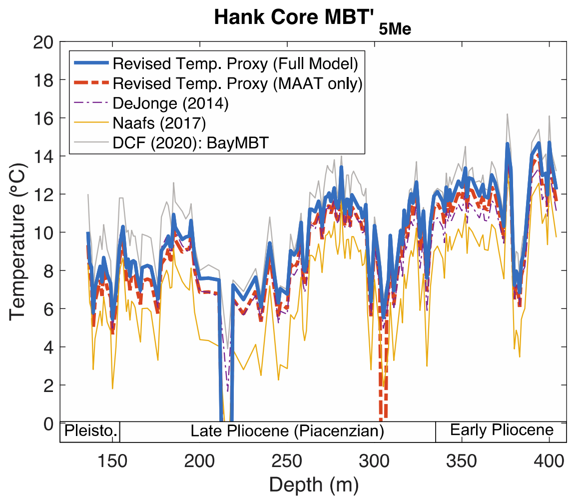

Fig. 5. Paleotemperature estimate for the Hank Core (Netherlands, northwestern Europe) using our revised nonlinear calibration for MBT'$_{5Me}$. The thick blue solid line shows the new nonlinear MAAT paleotemperature estimate using the calibration in Table 1, and the thick red dashed line shows the estimate using only the MAAT part of the model (excluding T_S and M). The 3 thin lines show results using previously published calibrations of De Jonge et al. (2014) (dashed-dotted purple), Naafs et al. (2017a) (yellow), and the BayMBT$_0$ model of Dearing Crampton-Flood et al. (2020) (gray). For this dataset, T_S = 7.1 °C and M = −23.9 mm, based on modern observations. Modeled MBT'$_{5Me}$ is interpolated from the predicted Eq. (7). See Code Availability for further details. We note that one point at 216 m depth plots off scale (less than 0 °C) due to a very low inferred MBT'$_{5Me}$ value of 0.324, which we believe may have been overcorrected for marine overprinting.

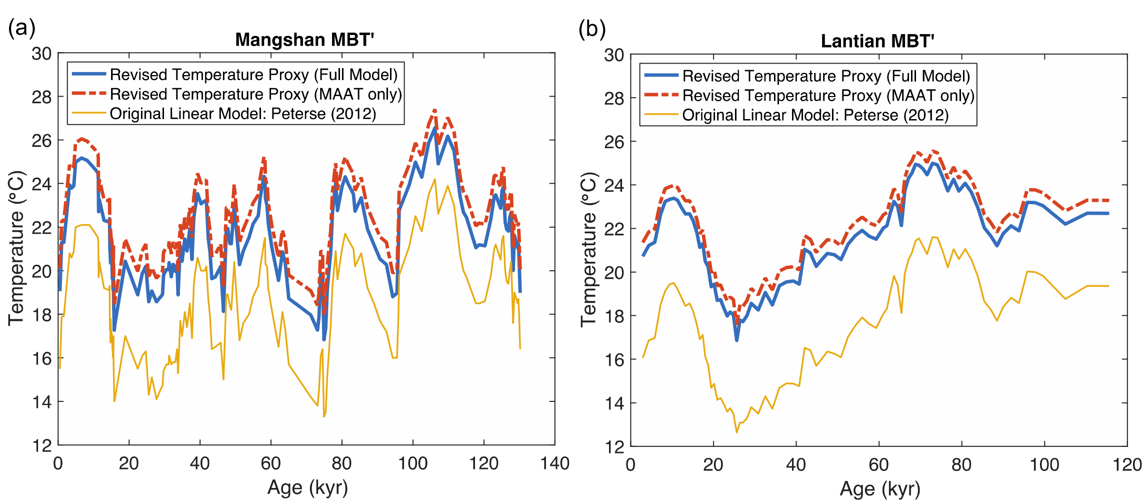

Fig. 6. Paleotemperature estimates using MBT' and CBT measurements for the (a) Mangshan loess profile and (b) Lantian loess profile. The blue thick solid lines show the MAAT paleotemperature estimates using the calibration in Table 1, the red thick dashed lines show the estimates using only the MAAT part of the model (using parameters m_0-m_3), and the thin yellow lines show the paleotemperature estimates using the standard MBT' calibration of Peterse et al. (2012). For Mangshan, T_S = 13.1 °C and M = 7.45 mm and for Lantian, T_S = 12.1 °C and M = -2.3 mm, based on modern observations. Soil moisture M has a negligible effect on the reconstructed temperature. For the revised estimates, modeled MAAT is interpolated from the predicted Eq. (7). See Code Availability for further details.

cancelling. We note that the recent calibration by Vequaud et al. (2022) produces estimates that are also similar to the De Jonge et al. (2014) calibration.

While many authors have moved away from using the MBT' proxy, the reduced RMSE from our nonlinear calibration suggests that it may still provide useful MAAT constraints (particularly from 18–25 °C) and we therefore also show a demonstration of the intermediate temperature bias for MBT'. In Fig. 6, we show two applications of the new model to paleosol records from Mangshan and Lantian, China (Peterse et al., 2014; Lu et al., 2016; see Fig. S2) which show that inferred temperatures are systematically higher than from standard MBT'/CBT calibrations (Peterse et al., 2012), with a maximum bias of about +4 °C from only the MAAT part of the new model (see red thick dashed curves in Fig. 6). Due to the nonlinearity, different temperatures have a different bias, with the +4 °C occurring during the coldest (glacial) periods and interglacials having a smaller +2–3 °C bias. This result has significant implications for the glacial-interglacial temperature differences at this site, with a smaller predicted ~5 °C glacial-to-interglacial warming, compared to previous estimates of ~6–10 °C over this time period at Mangshan (Peterse et al., 2014), Lantian (Gao et al., 2012) and Yuanbao (Jia et al., 2013) within the plateau (Fig. S3a). Our new estimate is consistent with the alkenone-based ~4.5 °C at Balikun Lake in Xinjiang (Zhao et al., 2017) and the 4–5 °C northern hemisphere integrated temperature change (Marcott et al., 2013, Shakun et al., 2012), although other recent studies suggest a somewhat larger ~7 °C warming of global mean surface temperature (Osman et al., 2021). Climate models also suggest that the annual temperatures during the Last Glacial Maximum were ~3–4 °C colder on the Chinese Loess Plateau relative to pre-industrial times (Tian and Jiang, 2016). We note that $\mathrm{MBT'}_{5\mathrm{Me}}$ results at Lantian do not have such a large systematic bias (and Mangshan does not have $\mathrm{MBT'}_{5\mathrm{Me}}$ measurements), but the $\mathrm{MBT'}_{5\mathrm{Me}}$ temperature reconstruction may be less accurate than MBT' results due to the high 6-methyl contribution there (~52.7 ± 7%; Lu et al., 2016; Naafs et al., 2017a,b) as well as the generally warm temperatures (see Section 4), and we therefore focus on the MBT' prediction. For the Mangshan and Lantian datasets, the seasonal bias is small compared to the MAAT bias, with an average bias in paleotemperature estimate of about −0.5 °C so that the overall bias is dominated by the strongly positive nonlinear curvature bias than by the weak seasonal bias.

6. CONCLUSIONS

We have shown that a new physical model for MBT-type temperature proxies improves upon standard empirical linear $\mathrm{MBT'}_{5\mathrm{Me}}$/MBT'-temperature calibrations by reducing biases due to saturation, seasonal temperature variability and moisture variability. Together, the new model accounts for up to 15 °C in estimated $\mathrm{MBT'}_{5\mathrm{Me}}$/MBT'-derived temperature biases in extreme cases, and using the new calibration decreases root mean squared errors compared with the linear calibrations. Initial applications show northwestern Europe Pliocene temperatures that are ~1 °C cooler than previous studies, and Last Glacial Maximum temperatures on the Chinese Loess Plateau that are ~2–4 °C warmer than previous calibrations. The physical constraints of the new nonlinear model and the improved errors compared to empirical models suggests that the nonlinear model has merit and may have wide applicability to other ratio-based temperature proxies.

7. CODE AVAILABILITY

MATLAB code to perform temperature estimates using the nonlinear models is provided on zenodo at https://doi.org/10.5281/zenodo.6363593.

Declaration of Competing Interest

The authors declare that they have no known competing financial interests or personal relationships that could have appeared to influence the work reported in this paper.

ACKNOWLEDGMENTS

This study was supported by the National Natural Science Foundation of China (Grant No. 41972188) and the National Science Foundation (Grant No. EAR-1762431). Author Contributions: J.Z. performed the laboratory experiments and compiled the datasets, V.C.T. designed the model, performed the data analysis and drafted the manuscript, Y.H. designed the initial study. All authors contributed to the writing and editing. We thank B.D. Naafs and two anonymous reviewers for their helpful comments.

APPENDIX A. SUPPLEMENTARY MATERIAL

Supplementary data to this article can be found online at https://doi.org/10.1016/j.gca.2022.04.022.

REFERENCES

Abatzoglou J., Dobrowski S., Parks S. and Hegewisch K. C. (2018) TerraClimate, a high-resolution global dataset of monthly climate and climatic water balance from 1958–2015. *Sci. Data* **5**, 170191.

Arfken G. (1985) *Mathematical Methods for Physicists*, third ed. Academic Press, New York.

Cao M., Rueda G., Rivas-Ruiz P., Trapote M. C., Henriksen M., Vegas-Vilarrúbia T. and Rosell-Melé A. (2018) Branched GDGT variability in sediments and soils from catchments with marked temperature seasonality. *Org. Geochem.* **122**, 98–114.

Dang X., Yang H., Naafs B. D. A., Pancost R. D., Evershed R. P. and Xie S. (2016) Direct evidence of moisture control on the methylation of branched glycerol dialkyl glycerol tetraethers in semi-arid and arid soils. *Geochim. Cosmochim. Acta* **189**, 24–36.

Dang X., Ding W., Yang H., Pancost R. D., Naafs B. D. A., Xue J., Lin X., Lu J. and Xie S. (2018) Different temperature dependence of the bacterial brGDGT isomers in 35 Chinese lake sediments compared to that in soils. *Org. Geochem.* **119**, 72–79.

De Jonge C., Hopmans E. C., Zell C. I., Kim J. H., Schouten S. and Sinninghe Damsté J. S. (2014) Occurrence and abundance of 6-methyl branched glycerol dialkyl glycerol tetraethers in soils: Implications for palaeoclimate reconstruction. *Geochim. Cosmochim. Acta* **141**, 97–112.

Dearing Crampton-Flood E., Tierney J. E., Peterse F., Kirkels F. M. S. A. and Sinninghe Damste J. S. (2020) BayMBT: A Bayesian calibration model for branched glycerol dialkyl glycerol tetraethers in soils and peats. *Geochim. Cosmochim. Acta* **268**, 142–159.

Dillon J. T., Lash S. J., Zhao J. J., Smith K. P., van Dommelen P., Scherer A. K. and Huang Y. (2018) Bacterial tetraether lipids in ancient bones record past climate conditions at the time of disposal. *J. Archaeol. Sci.* **96**, 45–56.

Dirghangi S. S., Pagani M., Hren M. T. and Tipple B. J. (2013) Distribution of glycerol dialkyl glycerol tetraethers in soils from two environmental transects in the USA. *Org. Geochem.* **59**, 49–60.

Fastovich D., Russell J. M., Jackson S. T. and Williams J. W. (2020) Deglacial temperature controls on no-analog community establishment in the Great Lakes Region. *Quat. Sci. Rev.* **234**, 106245.

Fenimore, C., Libert, J., Brill, M., 2000. Algebraic constraints implying monotonicity for cubics, *National Institute of Standards and Technology Interagency/Internal Report,* 6453.

Gao L., Nie J., Clemens S., Liu W., Sun J., Zech R. and Huang Y. (2012) The importance of solar insolation on the temperature variations for the past 110 kyr on the Chinese Loess Plateau. *Palaeogeogr. Palaeoclimatol. Palaeoecol.* **317**, 128–133.

Inglis G. N., Rohrssen M., Kennedy E. M., Crouch E. M. J., Raine I., Strogen D. P. B., Naafs D. A., Collinson M. E. and Pancost R. D. (2020) Terrestrial methane cycle perturbations during the onset of the Paleocene-Eocene Thermal Maximum. *Geology* **49** (5), 520–524.

Jia G. D., Rao Z. G., Zhang J., Li Z. Y. and Chen F. H. (2013) Tetraether biomarker records from a loess-paleosol sequence in the western Chinese Loess Plateau. *Front. Microbiol.* **4**, 199.

Karger D. N., Conrad O., Böhner J., Kawohl T., Kreft H., Soria-Auza R. W., Zimmermann N. E., Linder P. and Kessler M. (2017) Climatologies at high resolution for the Earth land surface areas. *Sci. Data* **4**, 170122.

Lauretano V., Kennedy-asser A. T., Korasidis V. A., Wallace M. W., Valdes P. J., Lunt D. J., Pancost R. D. and Naafs B. D. A. (2021) Eocene to Oligocene terrestrial Southern Hemisphere cooling caused by declining pCO_2. *Nat. Geosci.* **14**(9), 659–664.

Loomis S. E., Russell J. M., Ladd B., Street-Perrott F. A. and Sinninghe Damsté J. S. (2012) Calibration and application of the branched GDGT temperature proxy on East African lake sediments. *Earth Planet. Sci. Lett.* **357–358**, 277–288.

Lu H. X., Liu W. G., Wang H. Y. and Wang Z. (2016) Variation in 6-methyl branched glycerol dialkyl glycerol tetraethers in Lantian loess–paleosol sequence and effect on paleotemperature reconstruction. *Org. Geochem.* **100**, 10–17.

Lu H. X., Liu W. G., Yang H., Wang H. Y., Liu Z. H., Leng Q., Sun Y. B., Zhou W. J. and An Z. S. (2019) 800-kyr land temperature variations modulated by vegetation changes on Chinese Loess Plateau. *Nat. Commun.* **10**, 1958.

Marcott S. A., Shakun J. D., Clark P. U. and Mix A. C. (2013) A reconstruction of regional and global temperature for the past 11,300 Years. *Science* **339**, 1198–1201.

Martinez-Sosa P. and Tierney J. E. (2019) Lacustrine brGDGT response to microcosm and mesocosm incubations. *Org. Geochem.* **127**, 12–22.

Menges J., Huguet C., Alcañiz J. M., Fietz S., Sachse D. and Rosell-Melé A. (2014) Influence of water availability in the distributions of branched glycerol dialkyl glycerol tetraether in soils of the Iberian Peninsula. *Biogeosciences* **11**, 2571–2581.

Naafs B. D. A., Gallego-Sala A. V. and Pancost R. D. (2017a) Refining the global branched glycerol dialkyl glycerol tetraether (brGDGT) soil temperature calibration. *Org. Geochem.* **106**, 48–56.

Naafs B. D. A., Inglis G. N. and Pancost R. D. (2017b) Introducing global peat-specific temperature and pH calibrations based on brGDGT bacterial lipids. *Geochim. Cosmochim. Acta* **208**, 285–301.

Osman M. B., Tierney J. E., Zhu J., Tardif R., Hakim G. J., King J. and Poulsen C. J. (2021) Globally resolved surface temperatures since the Last Glacial Maximum. *Nature* **599**, 239–244.

Pearson E. J., Juggins S., Talbot H. M., Weckström J., Rosén P., Ryves D. B., Roberts S. J. and Schmidt R. (2011) A lacustrine GDGT-temperature calibration from the Scandinavian Arctic to Antarctic: Renewed potential for the application of GDGT-paleothermometry in lakes. *Geochim. Cosmochim. Acta* **75**, 6225–6238.

Peterse F., Pris M. A., Beets C. J., Troelstra S. R., Zheng H. B., Gu Z. Y., Schouten S. and Sinninghe Damsté J. S. (2011) Decoupled warming and monsoon precipitation in East Asia over the last deglaciation. *Earth Planet. Sci. Lett.* **301**, 256–264.

Peterse F., van der Meer J., Schouten S., Weijers J. W. H., Fierer N., Jackson R. B., Kim J. and Sinninghe Damsté J. S. (2012) Revised calibration of the MBT-CBT paleotemperature proxy based on branched tetraether membrane lipids in surface soils. *Geochim. Cosmochim. Acta* **96**, 215–229.

Peterse F., Martínez-García A., Zhou B., Beets C. J., Prins M. A., Zheng H. B. and Eglinton T. I. (2014) Molecular records of continental air temperature and monsoon precipitation variability in East Asia spanning the past 130,000 years. *Quat. Sci. Rev.* **83**, 76–82.

Raberg J. H., Harning D. J., Crump S. E., de Wet G., Blumm A., Kopf S., Geirsdottir A., Miller G. H. and Sepulveda J. (2021) Revised fractional abundances and warm-season temperatures substantially improve brGDGT calibrations in lake sediments. *Biogeosciences* **18**, 3579–3603.

Russell J. M., Hopmans E. C., Loomis S. E., Liang J. and Sinninghe Damsté J. S. (2018) Distributions of 5- and 6-methyl branched glycerol dialkyl glycerol tetraethers (brGDGTs) in East African lake sediment: Effects of temperature, pH, and new lacustrine paleotemperature calibrations. *Org. Geochem.* **117**, 56–69.

Shanahan T. M., Hughen K. A. and Van Mooy B. A. S. (2013) Temperature sensitivity of branched and isoprenoid GDGTs in Arctic lakes. *Org. Geochem.* **64**, 119–128.

Shakun J. D., Clark P. U., He F., Marcott S. A., Mix A. C., Liu Z. Y., Otto-Bliesner B., Schmittner A. and Bard E. (2012) Global warming preceded by increasing carbon dioxide concentrations during the last deglaciation. *Nature* **484**, 49–54.

Sun M., Yang S., Xiao J., Wang Y., Huang X., Zhang S., Yang X., Jiang W. and Ding Z. (2021) BrGDGTs-based temperature and hydrological reconstruction from fluvio-lacustrine sediments in the monsoonal North China Plain since 31 kyr BP. *Quat. Sci. Rev.*, 107268.

Tang C. Y., Yang H., Pancost R. D., Griffiths M. L., Xiao G. Q., Dang X. Y. and Xie S. C. (2017) Tropical and high latitude forcing of enhanced megadroughts in Northern China during the last four terminations. *Earth Planet. Sci. Lett.* **479**, 98–107.

Tian Z. P. and Jiang D. B. (2016) Revisiting last glacial maximum climate over China and East Asian monsoon using PMIP3 simulations. *Palaeogeogr. Palaeoclimatol. Palaeoecol.* **453**, 115–126.

Tierney J. E., Russell J. M., Eggermont H., Hopmans E. C., Verschuren D. and Sinninghe Damsté J. S. (2010) Environmental controls on branched tetraether lipid distributions in tropical East African lake sediments. *Geochim. Cosmochim. Acta* **74**, 4902–4918.

Vequaud P., Thibault A., Derenne S., Anquetil C., Collin S., Contreras S., Nottingham A. T., Sabatier P., Werne J. P. and Huguet A. (2022) FROG: A global machine-learning temperature calibration for branched GDGTs in soils and peats. *Geochim. Cosmochim. Acta* **318**, 468–494.

Wang H. Y., Liu W. G. and Lu H. X. (2016) Appraisal of branched glycerol dialkyl glycerol tetraether-based indices for North China. *Org. Geochem.* **98**, 118–130.

Weijers J. W. H., Schouten S., van den Donker J. C., Hopmans E. C. and Sinninghe Damsté J. S. (2007) Environmental controls on bacterial tetraether membrane lipid distribution in soils. *Geochim. Cosmochim. Acta* **71**(3), 703–713.

Weijers J. W. H., Bernhardt B., Peterse F., Werne J. P., Dungait J. A. J., Schouten S. and Sinninghe Damsté J. S. (2011) Absence of seasonal patterns in MBT–CBT indices in mid-latitude soils. *Geochim. Cosmochim. Acta* **75**, 3179–3190.

Zhao C., Rohling E., Liu Z. Y., Yang X. Q., Zhang E. L., Cheng J., Liu Z. H., An Z. S., Yang X. D., Feng X. P., Sun X. S., Zhang C., Yan T. L., Long H., Yan H., Yu Z. C., Liu W. G., Yu S. Y. and Chen J. (2021) Possible obliquity-forced warmth in southern Asia during the last glacial stage. *Sci. Bull.* **66**, 1136–1145.

Zhao J. J., An C. B., Huang Y. S., Morrill C. and Chen F. H. (2017) Contrasting early Holocene temperature variations between monsoonal East Asia and westerly dominated Central Asia. *Quat. Sci. Rev.* **178**, 14–23.

Zhao J. J., Huang Y., Yao Y., An Z., Zhu Y., Lu H. and Wang Z. (2020) Calibrating branched GDGTs in bones to temperature and precipitation: Application to Alaska chronological sequences. *Quat. Sci. Rev.* **240**, 106371.

Associate editor: Jessica Tierney